Journal of Physics: Conference Series **527** (2014) 012021 doi:10.1088/1742-6596/527/1/012021

Hybrid neutron stars with the field correlator method

Domenico Logoteta [1] **and Ignazio Bombaci** [2]

[1]Centro de Física Computacional, Department of Physics, University of Coimbra, 3004-516 Coimbra, Portugal
[2]Dipartimento di Fisica "Enrico Fermi", Università di Pisa and INFN Sezione di Pisa, Largo Bruno Pontecorvo 3, I-56127 Pisa, Italy

Abstract. We study the quark deconfinement phase transition in cold ($T = 0$) neutron star matter and we calculate various structural properties of hybrid stars. For the quark phase, we use an equation of state (EOS) based on the Field Correlator Method (FCM) extended to the case of nonzero baryon density. For the confined hadronic phase we use a relativistic mean field model considering both pure nucleonic and hyperonic matter. We constrain the values of the gluon condensate G_2, which is one of the EOS parameter within the FCM, making use of the measured mass, $M = 1.97 \pm 0.04\, M_\odot$, of the neutron star in PSR J1614-2230. Our results show that the values of G_2 extracted from the mass measurement of PSR J1614-2230 are consistent with the values of the same quantity derived, within the FCM, from recent lattice QCD calculations of the deconfinement transition temperature at zero baryon chemical potential.

1. Introduction

Neutron stars are the densest macroscopic objects in the universe. A large variety of calculations of neutron star structures [1, 2, 3, 4] predict a maximum stellar central density (the one for the maximum mass star configuration) in the range of $4 - 8$ times the saturation density ($\sim 2.8 \times 10^{14}$ g/cm^3) of nuclear matter. Therefore, neutron stars, can be viewed as natural laboratories to explore the low temperature T and high baryon chemical potential region of the phase diagram of quantum chromodynamics (QCD) [5, 6]. Under these conditions nonperturbative aspects of QCD are expected to play an essential role, and a transition to a phase with deconfined quarks and gluon is expected to occur and to effect a number of interesting astrophysical phenomena [7, 8, 9, 10, 11, 12, 13, 14, 15].

Current high-precision numerical calculations of QCD on a space-time lattice at zero baryon chemical potential μ_b (zero baryon density) seem to indicate that at high temperature and for physical values of the quark masses, the transition to quark gluon plasma is a crossover [16] rather than a real phase transition.

Unluckily, present lattice QCD calculations at finite baryon chemical potential are plagued with the so called "sign problem", which makes them unrealizable by all presently known lattice methods. Thus, in order to explore the QCD phase diagram at low temperature T and high μ_b, it is necessary to adopt some approximations in QCD or to apply some QCD effective model.

Along these lines the MIT bag model [17] and the Nambu Jona-Lasinio (NJL) model [18] have been widely used to calculate the quark matter EOS. However the MIT bag and the NJL

models (as other QCD effective models) can not make predictions in the high T and zero baryon chemical potential region and, thus, can not be tested with present lattice QCD calculations.

Recently the deconfinement phase transition has been described using an EOS of quark gluon plasma derived within the Field Correlator Method (FCM) [19, 20] extended to finite baryon chemical potential [21, 22]. The Field Correlator Method is a nonperturbative approach to QCD which includes from first principles the dynamics of confinement in terms of color electric and color magnetic correlators. The model contains two parameters: the gluon condensate G_2 and the large distance static quark-antiquark ($Q\bar{Q}$) potential V_1. These two quantities control the EOS of the denconfined phase at fixed quark masses and temperature. A very interesting aspect of the FCM is the possibility to describe the whole QCD phase diagram, from high temperature and low baryon chemical potential, to low T and high μ_b limit.

Another interesting feature of this method is that the value of the gluon condensate can be obtained from lattice QCD calculations of the deconfinement transition temperature T_c, at $\mu_b = 0$. This establishes a useful link to directly relate lattice QCD simulations and neutron star physics. To explore this link is the main aim of this work.

2. Equation of state of neutron star matter

The quark matter equation of state we used in this work is based on the Field Correlator Method (FCM) [19, 20]. The method has been recently extended to the case of nonzero baryon density [21, 22] making possible its application to neutron star matter.

The FCM provides a natural explanation and treatment of the dynamics of confinement in terms of Color Electric $D^E(x)$, $D_1^E(x)$ and Color Magnetic $D^H(x)$, $D_1^H(x)$ Gaussian correlators. In this work we use the approach described in Refs. [23, 24].

The EOS of the quark phase is governed by two parameters namely the static long distance $Q\bar{Q}$ potential V_1 and the gluon condensate G_2. All our results have been obtained in terms of these two quantities considered as independent on density [25, 26]. Recently in Ref. [27] a density dependence on G_2 has been proposed.

Using QCD sum rules [28], the gluon condensate G_2 has been determined, with large uncertainty, to be in the range $G_2 = (0.012 \pm 0.006)$ GeV^4. Therefore we have varied G_2 within the range determined in [28]. We used the following values of the current-quark masses: $m_u = m_d = 5$ MeV and $m_s = 150$ MeV. In summary, the quark matter EOS contains two parameters: G_2 and $V_1 = V_1(T = 0)$.

For the EOS of confined hadronic matter we adopt a nonlinear relativistic mean field model [29, 30] and we make use of the GM1 parametrization given by Glendening-Moszkoski [31, 32].

The nucleon coupling constants ($g_\sigma, g_\omega, g_\rho$) are fitted to the bulk properties of nuclear matter. In particular, for the GM1 parametrization [31, 32] the incompressibility of symmetric nuclear matter and the nucleon effective mass at the empirical saturation density are respectively $K = 300$ MeV and $M^* = 0.7\ M$ (being M the bare nucleon mass). The inclusion of hyperons involves new couplings, which can be written in terms of the nucleonic ones: $g_{\sigma Y} = x_\sigma g_\sigma$, $g_{\omega Y} = x_\omega g_\omega$, and $g_{\rho Y} = x_\rho g_\rho$. In this model it is assumed that all the hyperons in the baryon octet have the same coupling. We will consider x_σ in the range 0.6–0.8. In addition, following Ref. [31], we will take $x_\rho = x_\sigma$. Finally the binding energy of the Λ particle in symmetric nuclear matter, $B_\Lambda = -28$ MeV, is used to determine x_ω in terms of x_σ. Notice that the case with $x_\sigma = 0.6$ produces stars with a larger hyperon population (for a given stellar gravitational mass) with respect to the case $x_\sigma = 0.8$ [32, 33]. In addition to these two parametrizations for hyperonic matter (hereafter called NY matter), we will consider the case of pure nucleonic matter (hereafter called N matter).

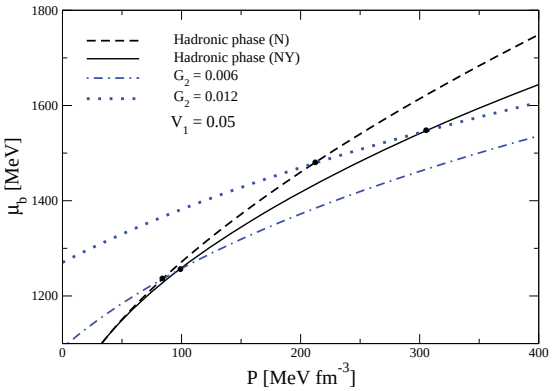

Figure 1. (Color online) Baryon chemical potential μ_b versus pressure P in β-stable matter at $T = 0$. Curves for the quark phase are relative to two different values of the gluon condensate G_2, reported in GeV^4, and $V_1 = 0.05$ GeV. Curves for the hadronic phase are relative to hyperonic matter (NY) with $x_\sigma = 0.7$ and to pure nucleonic matter (N).

3. Phase transition in beta-stable neutron star matter

The composition of neutron star matter is settled by the requirements of electric charge neutrality and equilibrium under the weak interaction processes (β-stable matter). Under such conditions and in the case of neutrino-free matter [1, 34], the chemical potential μ_i of each particle species i can be written in terms of two independent quantities, the baryonic and electric chemical potentials μ_b and μ_q respectively: $\mu_i = b_i\mu_b - q_i\mu_q$, where b_i is the baryon number of the species i and q_i denotes its charge in unit of the electron charge magnitude.

In the pure hadronic phase $\mu_b = \mu_n$, the neutron chemical potential, and $\mu_q = \mu_e$, the electron chemical potential. In the pure quark phase the quark chemical potentials μ_f (f=u, d, s) are related to μ_b and μ_q by the formulae $\mu_u = (\mu_b - 2\mu_q)/3$ and $\mu_d = \mu_s = (\mu_b + \mu_q)/3$.

We next assume a first order deconfinement phase transition [35] and require global electric charge neutrality of bulk beta-stable stellar matter [36]. An important consequence of imposing global charge neutrality is that the hadronic and the quark phases can coexist for a finite range of pressures. This treatment of the phase transition is known in the literature as the Gibbs construction for the mixed phase [36].

In the following we consider the case of $T = 0$ matter, which is appropriate to describe neutron stars interiors at times larger than about a few minutes after their formation [1, 34].

In figure 1 we plot the relation between the baryon chemical potential μ_b and the total (*i.e.* baryonic plus leptonic contributions) pressure P, in β-stable matter, for the hadron and the quark phases. For the hadronic phase we consider hyperonic matter (NY) with $x_\sigma = 0.7$ (continuous line) and pure nucleonic matter (N) (dashed line). For the quark phase we use two different values of the gluon condensate $G_2 = 0.006,\ 0.012$ GeV^4 and a common value $V_1 = 0.05$ GeV for the large distance static $Q\bar{Q}$ potential. The phase transition occurs at the intersection point between the curves describing the two different phases. This crossing point is significantly affected by the value of the gluon condensate, in particular when G_2 increases the onset of the deconfinement transition is shifted to higher pressure (higher baryon chemical potential). A similar qualitative behaviour is typical of bag-like models in terms of the bag constant B. In addition we note that the presence of hyperons in the hadronic phase moves the phase transition point to larger pressures. Similar results have been found using different values for the hyperon-nucleon couplings ($x_\sigma = 0.6,\ 0.8$) for the hadronic EOS.

Keeping a fixed value of the gluon condensate, $G_2 = 0.006$ GeV^4, we show in figure 2 the effects of V_1 on the phase transition point. As one can see, increasing the value of V_1 the

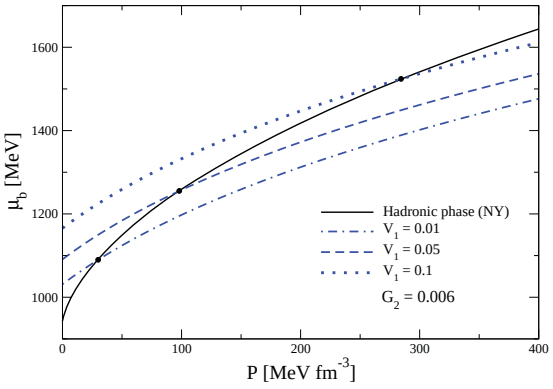

Figure 2. (Color online) Baryon chemical potential μ_b versus P in β-stable matter at $T = 0$. Curves for the quark phase are relative to three different values of V_1, reported in GeV, and for $G_2 = 0.006$ GeV^4. The curve for the hadronic phase is relative to hyperonic matter (NY) with $x_\sigma = 0.7$.

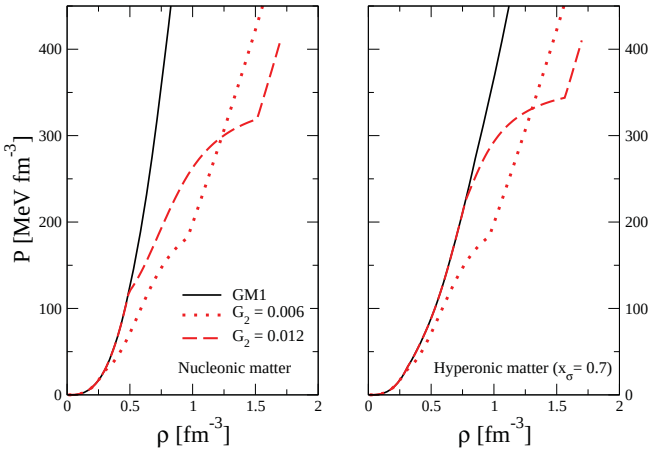

Figure 3. (Color online) Total pressure P of cold β-stable matter as a function of the baryon number density ρ, for different values of G_2 (reported in GeV^4 units) and for $V_1 = 0.05$ GeV. In the left (right) panel we show results for pure nucleonic (hyperonic) matter in the hadronic phase. For the hyperonic matter EOS we set $x_\sigma = 0.7$.

transition point is shifted to values of the pressure higher and higher.

In figure 3, we show the pressure for β-stable matter as a function of the baryon number density ρ in the case of pure nucleonic matter (left panel) and hyperonic matter (right panel) with $x_\sigma = 0.7$ for the hadronic phase. For the quark phase we consider two different values of the gluon condensate G_2. Increasing the value of G_2 we note a shift of the phase transition to larger baryon densities. This is consistent with the behaviour of figure 1.

4. Hybrid star structure

In this section we show the results of our calculations of hybrid stars structure. To this purpose we integrate the well known Tolman, Oppenheimer and Volkov equations (see *e.g.* [32, 37]) to get various stellar properties and report the results of a systematic study in which we vary the value of the gluon condensate G_2 between the constraints imposed by QCD sum rules [28]. To

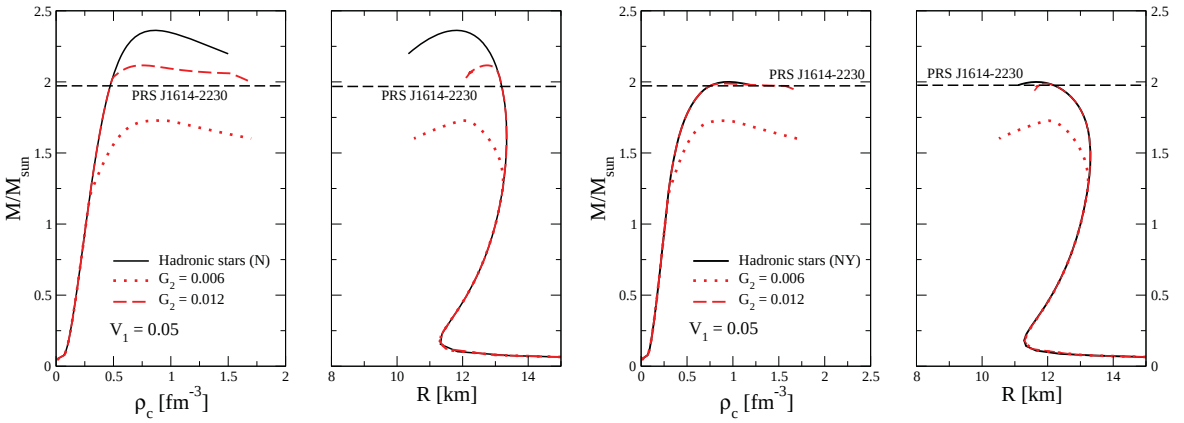

Figure 4. (Color online) Stellar mass M versus central baryon number density ρ_c (first and third panels) and versus stellar radius R (second and fourth panels) for hybrid stars for two values of G_2 (reported in GeV^4 units) and for $V_1 = 0.05$ GeV. Continuous lines in each panel denote compact stars with no quark matter content. The first two panels refer to the pure nucleonic matter case (N) while in third and fourth panels refer the hyperonic matter case (NY) with $x_\sigma = 0.7$. The dashed horizontal line, in each panel, represents the measured mass of PSR J1641-2230.

model the stellar crust we have used the EOS of Ref. [38].

In figure 4 we report the stellar gravitational mass M (in unit of the solar mass $M_\odot = 1.99 \times 10^{33}$g) versus the central baryon number density ρ_c (first and third panels) and M versus radius R (second and fourth panels) in the case of pure nucleonic stars (continuous lines) and of hybrid stars for different G_2. The dashed horizontal line, in each panel, represents the mass of the PSR J1641-2230 ($M = 1.97 \pm 0.04\, M_\odot$) [39]. We first focus on the first two panels of figure 4, where in the hadronic phase just nucleons are included. We obtain stable hybrid star configurations for all the considered values of the gluon condensate, with maximum masses ranging from $M_{max} = 1.72\, M_\odot$ (case with $G_2 = 0.006$ GeV^4) to $M_{max} = 2.11\, M_\odot$ ($G_2 = 0.012$ GeV^4). Notice that the hybrid star branch of the stellar equilibrium configurations shrinks as G_2 is increased. This is in full agreement with the results for the EOS reported in figure 3.

We now turn to the case (third and fourth panels in figure 4) in which the hadronic phase contains hyperons (NY matter) and we set $x_\sigma = 0.7$. Notice that the presence of hyperons reduces the value of the maximum mass of pure hadronic star (*i.e.* compact stars with no quark matter content) from $M_{max} = 2.33\, M_\odot$ in case of pure nucleonic stars (continuous line in the first and second panels of figure 4) to $M_{max} = 1.99\, M_\odot$ in case of hyperonic stars with $x_\sigma = 0.7$ (continuous line in the third and fourth panels in figure 4). We obtain stable hybrid star configurations also in the case of NY matter for all the considered values of the gluon condensate and, similarly to the nucleonic case, we note again that the hybrid star branch shrinks as G_2 is increased. In this case we get maximum hybrid star masses of 1.72 $M_\odot$ for $G_2 = 0.006$ GeV^4 and 1.98 $M_\odot$ for $G_2 = 0.012$ GeV^4. We note that for values of the gluon condensate $G_2 > 0.012$ GeV^4 our models are able to predict the mass of the PSR J1614-2230. More precisely, the minimum value of G_2 required for the pure nucleonic case is $G_2 = 0.010$ GeV^4 while for the hyperonic case such value is $G_2 = 0.012$ GeV^4. It should be noted that these values of G_2 depend besides the EOS of hadronic matter, on the value adopted for the large distance $Q\bar{Q}$ potential.

In table 1 we report the properties of the maximum mass configuration for hybrid stars for $V_1 = 0.01$ GeV and varying G_2 and the hyperon coupling constants. We note that in the case $x_\sigma = 0.6$, hybrid stars are possible only for $G_2 < 0.013$ GeV^4. In fact, for $G_2 > 0.013$ GeV^4 the

Table 1. Properties of the maximum mass configuration for hybrid stars for different values of the gluon condensate G_2 in GeV^4 (second column) and for $V_1 = 0.01$ GeV. The parameter x_σ (first column) fixes the hyperons coupling constants as described in section 2. The entry N in the first column refers to the case of pure nucleonic matter for the hadronic phase. The mass M_{max}, the central baryon number density ρ_c^{Hyb} and the radius R of the maximum mass configuration are reported respectively in the third, fourth and fifth column. The quantities with the label HS refer to the case of purely hadronic stars. Stellar masses are reported in unit of the solar mass $M_\odot = 1.99 \times 10^{33}$g, central densities are given in fm^{-3}, and stellar radii in km.

x_σ	G_2	M_{max}	ρ_c^{Hyb}	R	M_{max}^{HS}	ρ_c^{HS}	R^{HS}
	0.006	1.44	1.55	9.54			
N	0.012	1.89	0.77	12.55	2.33	0.87	11.70
	0.016	2.05	0.75	12.66			
	0.006	1.44	1.56	9.52			
0.8	0.012	1.89	0.77	12.53	2.15	0.94	11.50
	0.016	2.04	0.81	12.40			
	0.006	1.43	1.56	9.51			
0.6	0.010	1.73	0.89	12.00	1.80	1.00	11.49
	0.013	1.80	1.00	11.49			

baryon number density for the onset of the mixed phase is larger than the central baryon number density of the maximum mass pure hadronic star. Notice that for $x_\sigma = 0.6$ is not possible to account for the measured mass of PSR J1614-2230 for any value of G_2.

5. Lattice QCD calculations and measured neutron star masses

Within the FCM the deconfinement transition temperature T_c at $\mu_b = 0$ reads [21]

$$T_c = \frac{a_0}{2} G_2^{1/4} \left(1 + \sqrt{1 + \frac{V_1(T_c)}{2 a_0 G_2^{1/4}}} \right), \tag{1}$$

with $a_0 = (3\pi^2/768)^{1/4}$ in the case of three flavors.

In their analysis authors of Ref. [21] assume $V_1(T_c) = 0.5$ GeV, thus T_c in equation (1) is a simple function of G_2, and is represented in figure 5 by the curve labeled $V_1(T_c) = 0.5$ GeV. This result can hence be compared with lattice QCD calculations of T_c giving the possibility to extract the range of values for the gluon condensate compatible with lattice results. This comparison has been done in Ref. [21], and it is done in the present work in figure 5, where we consider recent lattice QCD calculations of T_c [40, 41]. Details to the specific lattice QCD calculations are given in the figure 5 caption. As one can see, the comparison with lattice QCD calculations of T_c restricts the gluon condensate in a rather narrow range $G_2 = 0.0025$–0.0050 GeV^4.

Next to verify if these values of G_2 are compatible with those extracted in section 4 from hybrid star calculations and measured neutron star masses, we need to relate the parameter $V_1 \equiv V_1(0)$, entering in the zero temperature EOS of the quark phase, with $V_1(T_c)$ in equation (1).

In Ref. [23] it has been shown that such relation is given by:

$$V_1(T) = V_1(0) \left\{ 1 - \frac{3}{2} \frac{\lambda T}{\hbar c} + \frac{1}{2} \left(1 + 3 \frac{\lambda T}{\hbar c} \right) e^{-\frac{\hbar c}{\lambda T}} \right\}, \tag{2}$$

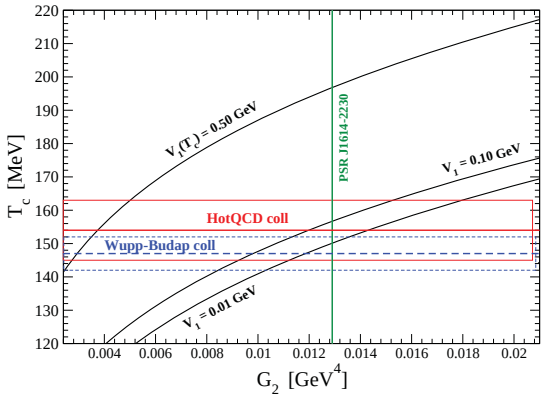

Figure 5. (Color online) Deconfinement transition temperature T_c at $\mu_b = 0$. The curve labeled with $V_1(T_c) = 0.5$ GeV reproduces the FCM results of Ref. [21] for a fixed value $V_1(T_c) = 0.5$ GeV of the large distance static $Q\bar{Q}$ potential. The curve labeled with $V_1 = 0.01$ GeV ($V_1 = 0.10$ GeV) corresponds to the transition temperature at $\mu_b = 0$ obtained solving numerically equations (1) and (2) for the case $V_1(0) = 0.01$ GeV ($V_1(0) = 0.10$ GeV). The horizontal heavy and thin lines represent respectively the central value and the error estimate of lattice QCD calculations. In particular, the (red) continuous lines refer to the calculations [41] of the HotQCD collaboration $T_c = (154 \pm 9)$ MeV; the (blue) short-dashed lines refer to the calculations [40] of the Wuppertal–Budapest collaboration $T_c = (147 \pm 5)$ MeV. Finally, the vertical green line represents the lower limit for G_2 which is compatible with the lower bound of the measured mass of PSR J1614-2230 for the case $V_1(0) = 0.01$ GeV.

where $\lambda = 0.34$ fm [42] is the vacuum correlation length. Thus $V_1(T_c) = 0.5$ GeV corresponds to $V_1(0) = 0.85$ GeV to be used in the $T = 0$ EOS of the quark phase. In this case there is no phase transition in neutron stars for all the considered values of G_2. Thus for these values of the EOS parameters PSR J1614-2230 would be a pure nucleonic star.

We can also evaluate the FCM transition temperature at $\mu_b = 0$ corresponding to the case $V_1(0) = 0.01$ GeV. To this purpose we solve numerically equations (1)–(2) and we obtain the results represented in figure 5 by the curve labeled $V_1 = 0.01$ GeV. The comparison of these results with lattice QCD calculations [40, 41] of T_c restricts the gluon condensate in the range $G_2 = 0.0103$–0.0180 GeV^4. Coming now to the astrophysical constraints on the gluon condensate, the vertical grey line in figure 5 represents the lower limit for G_2 which is compatible, in the case $V_1(0) = 0.01$ GeV, with the lower bound of the measured mass of PSR J1614-2230 (see section 4).

A similar analysis can be done for the case $V_1(0) = 0.10$ GeV. Now the comparison between the FCM transition temperature at $\mu_b = 0$ (curve labeled $V_1 = 0.10$ GeV in figure 5) and lattice QCD calculations of the same quantity gives $G_2 = 0.0085$–0.0153 GeV^4, whereas one gets $G_2 \geq 0.006$ GeV^4 from the lower bound of the measured mass of PSR J1614-2230.

We thus find that the values of the gluon condensate extracted within the FCM from lattice QCD calculations of the deconfinement transition temperature T_c at $\mu_b = 0$ are fully compatible with the value of the same quantity extracted from measured neutron star masses.

6. Summary and conclusions

In this work we have studied the quark deconfinement phase transition in neutron star matter and the properties of hybrid stars employing an EOS for the quark phase derived from the FCM extended to finite baryon chemical potential. The EOS of the FCM is parametrized in terms of the gluon condensate G_2 and of the large distance static $Q\bar{Q}$ potential V_1 at zero temperature.

We have obtained stable hybrid star configurations for all the values of the gluon condensate fulfilling the condition that the deconfinement transition can occur in pure hadronic stars.

We have established that the values of the gluon condensate extracted within the FCM from lattice QCD calculations of the deconfinement transition temperature at $\mu_b = 0$, are fully consistent with the value of the same quantity constrained by the mass measurement of PSR J1614-2230. The FCM thus provides a powerful tool to link numerical calculations of QCD on a space-time lattice with neutron stars physics.

References

[1] Prakash M, Bombaci I, Prakash M, Ellis P J, Lattimer J M, and Knorren R 1997 *Phys. Rep.* **280** 1
[2] Datta B, Thampan A V, and Bombaci I 1998 *Astron. and Astrophys.* **334** 943
[3] Lattimer J M and Prakash M 2001 *Astrophys. J.* **550** 426
[4] Peng G X, Li A, and Lombardo U 2008 *Phys. Rev. C* **77** 065807
[5] Alford M G, Schmitt A, Rajagopal K, and Schafer T 2008 *Rev. Mod. Phys.* **80** 1455
[6] Anglani R, Casalbuoni R, Ciminale M, Ippolito N, Gatto R, Mannarelli M, and Ruggieri M 2014 *Rev. Mod. Phys.* (to be published); `arXiv:1302.4264`
[7] Perez-Garcia M A, Silk J, and Stone J R 2010 *Phys. Rev. Lett.* **105** 141101
[8] Li X D, Ray S, Dey J, Dey M, and Bombaci I 1999 *Astrophys. J.* **527** L51
[9] Sotani H, Yasutake N, Maruyama T, and Tatsumi T 2011 *Phys. Rev. D* **83** 024014
[10] Berezhiani Z, Bombaci I, Drago A, Frontera F, and Lavagno A 2003, *Astrophys. J.* **586** 1250; Bombaci I, Parenti I, and Vidaña I 2004 *Astrophys. J.* **614** 314
[11] Lugones G and Bombaci I 2005 *Phys. Rev. D* **72** 065021; Bombaci I, Lugones G, and Vidaña I 2007 *Astron. and Astrophys.* **462** 1017
[12] Bombaci I, Logoteta D, Providência C, and Vidaña I 2011 *Astron. and Astrophys.* **528** A71
[13] Logoteta D, Providência C, Vidaña I, and Bombaci I 2012 *Phys. Rev. C* **85** 055807
[14] Weissenborn S, Sagert I, Pagliara G, Hempel M, and Schaffner-Bielich J 2011 *Astrophys. J.* **740** L14
[15] Bhattacharyya S, Thampan A V, and Bombaci I 2001 *Astron. and Astrophys.* **372** 925
[16] Aoki Y, Endrodi G, Fodor Z, Katz S D, and Szabó K K 2006 *Nature* **443** 675
[17] Chodos A *et al.* 1974 *Phys. Rev. D* **9** 3471; Farhi E and Jaffe R L 1984 *Phys. Rev. D* **30** 272
[18] Nambu Y and Jona-Lasinio G 1961 *Phys Rev.* **122** 345
[19] Dosh H G 1987 *Phys. Lett. B* **190** 177; Dosh H G and Simonov Yu A 1988 *Phys. Lett. B* **205** 339; Simonov Yu A 1988 *Nucl. Phys. B* **307** 512
[20] Di Giacomo A, Dosch H G, Shevchenko V I, and Simonov Yu A 2002 *Phys. Rep.* **372** 319
[21] Simonov Yu A and Trusov M A 2007 *Phys. Lett. B* **650** 36
[22] Komarov E V and Simonov Yu A 2008 *Ann. Phys.* **323** 1230
[23] Bombaci I and Logoteta D 2013 *MNRAS Letters* **L79** 433
[24] Logoteta D and Bombaci I 2013 *Phys. Rev. D* **88** 063001
[25] Baldo M, Burgio G F, Castorina P, Plumari S, and Zappalà D 2008 *Phys. Rev. D* **78** 063009
[26] Pereira F I M 2011 *Nucl. Phys. A* **860** 102; 2013 *Nucl. Phys. A* **897** 151
[27] Plumari S, Burgio G F, Greco V, and Zappalá D 2013 *Phys. Rev. D* **88** 083005
[28] Shifman M A, Vainshtein A I, and Zakharov V I 1979 *Nucl. Phys. B* **147** 385; *Nucl. Phys. B* **147** 448
[29] Walecka J D 1974 *Ann. Phys. (N.Y.)* **83** 491; Serot B D and Walecka J D 1986 *Adv. Nucl. Phys.* **16** 1
[30] Boguta J and Bodmer A R 1977 *Nucl. Phys. A* **292** 413
[31] Glendening N K and Moszkowski S 1991 *Phys. Rev. Lett.* **67** 2414
[32] Glendenning N K 2000 *Compact Stars, Nuclear Physics, Particle Physics, and General Relativity* (Springer, New York)
[33] Bombaci I, Panda P K, Providência C, and Vidaña I 2008 *Phys. Rev. D* **77** 083002
[34] Bombaci I, Prakash M, Prakash M, Ellis P J, Lattimer J M, and Brown G E 1995 *Nucl. Phys. A* **583** C623
[35] Fodor Z and Katz S D 2004 *J. High Energy Phys.* **04** 050
[36] Glendening N K 1992 *Phys. Rev. D* **46** 1274
[37] Haensel P, Potekhin A Y, and Yakovlev D G 2007 *Neutron Stars 1: Equation of State and Structure* (Springer)
[38] Baym G, Pethick C, and Sutherland D 1971 *Astrophys. J.* **170** 299; Negele J W and Vautherin D 1973 *Nucl. Phys. A* **207** 298
[39] Demorest P, Pennucci T, Ransom S, Roberts M, and Hessels J 2010 *Nature* **467** 1081
[40] Borsanyi S *et al.* 2010 *J. High Energy Phys.* **09** 073
[41] Bazavov A *et al.* 2012 *Phys. Rev. D* **85** 054503
[42] D'Elia M, Di Giacomo A, and Meggiolaro E 1997 *Phys. Lett. B* **408** 315